JOURNAL OF COMPUTATIONAL PHYSICS 53, 382–394 (1984)

Solution of Elliptic Equations Using Fast Poisson Solvers

PAUL A. BERNHARDT AND J. U. BRACKBILL

Los Alamos National Laboratory,
Los Alamos, New Mexico 87545

Received August 10, 1982; revised July 22, 1983

Certain nonseparable elliptic equations may be transformed into a sequence of Poisson equations. The solutions of these equations are efficiently found using fast Poisson solvers. The method is illustrated by solving for the internal electric potential in convecting plasma clouds.

1. INTRODUCTION

In a recent review article by Detyna [4], it is stated that there are "no rapid elliptic solvers (RES) capable of solving a general nonseparable elliptic partial differential equation (EPDE) in 2- or 3-dimensions." There exist, however, RES which may be applied to general separable EPDEs. It is the purpose of this paper to show that linear self-adjoint EPDEs have a series solution or have an iterative solution such that each term in the solution is described by a separable EPDE. RES in the form of fast Poisson solvers provide these terms. The solution procedure, which is an extension of the method described in Brackbill and Forslund [1], is illustrated with an example of the internal electric potential associated with nonlinear plasma transport.

2. DERIVATION OF THE RECURSIVE SERIES

Consider the self-adjoint, nonseparable generalization of Poisson's equation in two dimensions

$$\frac{\partial}{\partial x}\left[A(x, y)\frac{\partial}{\partial x}\phi_0(x, y)\right] + \frac{\partial}{\partial y}\left[B(x, y)\frac{\partial}{\partial y}\phi_0(x, y)\right] = S_0(x, y), \tag{1}$$

where $\phi_0(x, y)$ is the unknown function. A and B are nonzero functions with the same sign. Depending on boundary condition (Dirichlet, Neumann, periodic, or mixed) $S_0(x, y)$ may have to satisfy certain compatibility conditions.

Equation (1), in general, cannot be solved directly with rapid elliptic solvers. The solution of (1) is based on (1) splitting the derivatives into curl-free and gradient-free parts and (2) using the identities $\nabla \times \nabla\psi = 0$ and $\nabla \cdot \nabla \times \bar{\phi} = 0$ to isolate terms.

0021-9991/84 $3.00

In two dimensions, we define the functions ϕ_0, ϕ_1, and ψ_0 by

$$A\frac{\partial\phi_0}{\partial x}=\frac{\partial\psi_0}{\partial x}+\frac{\partial\phi_1}{\partial y}, \tag{2a}$$

$$B\frac{\partial\phi_0}{\partial y}=\frac{\partial\psi_0}{\partial y}-\frac{\partial\phi_1}{\partial x}. \tag{2b}$$

Substitution of (2a) and (2b) into (1) yields Poisson's equation,

$$\frac{\partial^2\psi_0}{\partial x^2}+\frac{\partial^2\psi_0}{\partial y^2}=S_0(x, y). \tag{3}$$

The equation for ϕ_1 is found by equating expressions for $\partial^2\phi_0/\partial x\,\partial y$ obtained from (2a) and (2b),

$$\frac{\partial^2\phi_0}{\partial x\,\partial y}=\frac{\partial}{\partial y}\left(\frac{1}{A}\frac{\partial\psi_0}{\partial x}\right)+\frac{\partial}{\partial y}\left(\frac{1}{A}\frac{\partial\phi_1}{\partial y}\right)=\frac{\partial}{\partial x}\left(\frac{1}{B}\frac{\partial\psi_0}{\partial y}\right)-\frac{\partial}{\partial x}\left(\frac{1}{B}\frac{\partial\phi_1}{\partial x}\right). \tag{4}$$

Equation (4) is rewritten as

$$\frac{\partial}{\partial x}\left(A^*\frac{\partial\phi_1}{\partial x}\right)+\frac{\partial}{\partial y}\left(B^*\frac{\partial\phi_1}{\partial y}\right)=S_1(x, y), \tag{5}$$

where $A^*=1/B$, $B^*=1/A$, and

$$S_1(x, y)=\frac{\partial}{\partial x}\left(A^*\frac{\partial\psi_0}{\partial y}\right)-\frac{\partial}{\partial y}\left(B^*\frac{\partial\psi_0}{\partial x}\right).$$

Equation (5) is of the same form as Eq. (1). A substitution similar to Eqs. (2a) and (2b), i.e.,

$$A^*\frac{\partial\phi_1}{\partial x}=\frac{\partial\psi_1}{\partial x}+\frac{\partial\phi_2}{\partial y}, \tag{6a}$$

$$B^*\frac{\partial\phi_1}{\partial y}=\frac{\partial\psi_1}{\partial y}-\frac{\partial\phi_2}{\partial x}, \tag{6b}$$

yields another Poisson's equation for ψ_1,

$$\frac{\partial^2\psi_1}{\partial x^2}+\frac{\partial^2\psi_1}{\partial y^2}=S_1(x, y), \tag{7}$$

and another generalized Poisson's equation for ϕ_2,

$$\frac{\partial}{\partial x}\left(A\frac{\partial\phi_2}{\partial x}\right)+\frac{\partial}{\partial y}\left(B\frac{\partial\phi_2}{\partial y}\right)=S_2(x, y), \tag{8}$$

where

$$S_2(x, y) = \frac{\partial}{\partial x}\left(A\frac{\partial \psi_1}{\partial y}\right) + \frac{\partial}{\partial y}\left(B\frac{\partial \psi_1}{\partial x}\right).$$

Substitution of (6a) and (6b) into (2a) and (2b) yields

$$\frac{\partial \phi_0}{\partial x} = \frac{1}{A}\left\{\frac{\partial \psi_0}{\partial x} + A\left[\frac{\partial \psi_1}{\partial y} - \frac{\partial \phi_2}{\partial x}\right]\right\}, \tag{9a}$$

$$\frac{\partial \phi_0}{\partial y} = \frac{1}{B}\left\{\frac{\partial \psi_0}{\partial y} - B\left[\frac{\partial \psi_1}{\partial x} + \frac{\partial \phi_2}{\partial y}\right]\right\}. \tag{9b}$$

This process is continued to produce an infinite series solution for the derivatives of ϕ_0,

$$\frac{\partial \phi_0}{\partial x} = \sum_{n=0}^{\infty} (-1)^n \left[\frac{1}{A}\frac{\partial \psi_{2n}}{\partial x} + \frac{\partial \psi_{2n+1}}{\partial y}\right], \tag{10a}$$

$$\frac{\partial \phi_0}{\partial y} = \sum_{n=0}^{\infty} (-1)^n \left[\frac{1}{B}\frac{\partial \psi_{2n}}{\partial y} - \frac{\partial \psi_{2n+1}}{\partial x}\right]. \tag{10b}$$

The functions ψ_m are calculated recursively from Poisson's equation,

$$\frac{\partial^2 \psi_m}{\partial x^2} + \frac{\partial^2 \psi_m}{\partial y^2} = S_m \qquad \{m = 0, 1, 2,...\}, \tag{11a}$$

where S_0 is initially specified,

$$S_{2n} = \frac{\partial}{\partial x}\left(A\frac{\partial \psi_{2n-1}}{\partial y}\right) - \frac{\partial}{\partial y}\left(B\frac{\partial \psi_{2n-1}}{\partial x}\right) \qquad \{n = 1, 2, 3,...\}, \tag{11b}$$

and

$$S_{2n+1} = \frac{\partial}{\partial x}\left(\frac{1}{B}\frac{\partial \psi_{2n}}{\partial y}\right) - \frac{\partial}{\partial y}\left(\frac{1}{A}\frac{\partial \psi_{2n}}{\partial x}\right) \qquad \{n = 0, 1, 2, 3,...\}. \tag{11c}$$

Values of ψ_m $(m = 0, 1, 2, 3...)$ may be obtained from Eq. (11) by using rapid elliptic solvers. Derivatives of each succeeding $\psi_m(x, y)$ are computed numerically and summed according to Eqs. (10a) and (10b) until convergence is achieved. RMS convergence criteria which have been tested in our numerical examples use the error measure,

$$\varepsilon_x^2 = \iint \left[\frac{1}{A}\frac{\partial \psi_{2n}}{\partial x} - \frac{\partial \psi_{2n-1}}{\partial y}\right]^2 dx\, dy \Big/ \iint \left[\frac{\partial \phi_{0n}}{\partial x}\right]^2 dx\, dy, \tag{12}$$

$$\varepsilon_y^2 = \iint \left[\frac{1}{B}\frac{\partial \psi_{2n}}{\partial y} + \frac{\partial \psi_{2n-1}}{\partial x}\right]^2 dx\, dy \Big/ \iint \left[\frac{\partial \phi_{0n}}{\partial y}\right]^2 dx\, dy, \tag{13}$$

where the integrals over x and y are numerical sums over the coordinate grid and ϕ_{0n} is the potential defined by (10a) and (10b) summed to n terms. The quantities in the

brackets in the numerators of (12) and (13) are constructed from the second term for $n-1$ and the first terms for n in the series given by (10a) and (10b). Computation of the summation continues until the $\sqrt{\varepsilon_x^2+\varepsilon_y^2}<\varepsilon$, where ε is much less than unity.

3. Derivation of the Iterative Solution

As an alternative to an infinite series solutions, an iterative solution is derived. The substitution,

$$A\frac{\partial \phi_0}{\partial x}=\frac{\partial u}{\partial x}+A\frac{\partial v}{\partial y}, \tag{14a}$$

$$B\frac{\partial \phi_0}{\partial y}=\frac{\partial u}{\partial y}-B\frac{\partial v}{\partial x}, \tag{14b}$$

into Eq. (1) yields

$$\frac{\partial^2 u}{\partial x^2}+\frac{\partial^2 u}{\partial y^2}=S_0(x,y)-\frac{\partial}{\partial x}\left(A\frac{\partial v}{\partial y}\right)+\frac{\partial}{\partial y}\left(B\frac{\partial v}{\partial x}\right). \tag{15}$$

Dividing Eq. (14a) by A and differentiating with respect to y yields

$$\frac{\partial^2 \phi_0}{\partial x\,\partial y}=\frac{\partial}{\partial y}\left(\frac{1}{A}\frac{\partial u}{\partial x}\right)+\frac{\partial^2 v}{\partial y^2}. \tag{16a}$$

Similarly, Eq. (14b) becomes

$$\frac{\partial^2 \phi_0}{\partial x\,\partial y}=\frac{\partial}{\partial x}\left(\frac{1}{B}\frac{\partial u}{\partial y}\right)-\frac{\partial^2 v}{\partial x^2}. \tag{16b}$$

Equating (16a) and (16b) gives

$$\frac{\partial^2 v}{\partial x^2}+\frac{\partial^2 v}{\partial y^2}=-\frac{\partial}{\partial y}\left(\frac{1}{A}\frac{\partial u}{\partial x}\right)+\frac{\partial}{\partial x}\left(\frac{1}{B}\frac{\partial u}{\partial y}\right). \tag{17}$$

Eqs. (15) and (17) form the basis for the iteration. Let $u_n(x,y)$ and $v_n(x,y)$ be the values for $u(x,y)$ and $v(x,y)$ at iteration step n. Initially, $u_0(x,y)=0$ and $v_0(x,y)=0$. The solution is found from the equations,

$$\frac{\partial^2 u_{n+1}}{\partial x^2}+\frac{\partial^2 u_{n+1}}{\partial y^2}=S_0(x,y)-(A-B)\frac{\partial^2 v_n}{\partial x\,\partial y}+\frac{\partial A}{\partial x}\frac{\partial v_n}{\partial y}+\frac{\partial B}{\partial y}\frac{\partial v_n}{\partial x}, \tag{18a}$$

$$\frac{\partial^2 v_{n+1}}{\partial x^2}+\frac{\partial^2 v_{n+1}}{\partial y^2}=-\frac{(A-B)}{AB}\frac{\partial^2 u_{n+1}}{\partial x\,\partial y}-\frac{\partial\left(\frac{1}{A}\right)}{\partial y}\frac{\partial u_{n+1}}{\partial x}+\frac{\partial\left(\frac{1}{B}\right)}{\partial x}\frac{\partial u_{n+1}}{\partial y}. \tag{18b}$$

Note that the left side of Eqs. (18a) and (18b) are Poisson's equations. At each step in the iteration, the new estimates for ϕ_0 are given by

$$\frac{\partial \phi_{0n}}{\partial x} = \frac{1}{A}\frac{\partial u_n}{\partial x} + \frac{\partial v_n}{\partial y}, \tag{19a}$$

$$\frac{\partial \phi_{0n}}{\partial y} = \frac{1}{B}\frac{\partial u_n}{\partial y} - \frac{\partial v_n}{\partial x}. \tag{19b}$$

The convergence criteria for the iteration is similar to the one for the series. Define the RMS error as

$$\varepsilon_x^2 = \iint \left[\frac{\partial \phi_{0n}}{\partial x} - \frac{\partial \phi_{0n-1}}{\partial x}\right]^2 dx\,dy \Big/ \iint \left[\frac{d\phi_{0n}}{\partial x}\right]^2 dx\,dy, \tag{20a}$$

$$\varepsilon_y^2 = \iint \left[\frac{\partial \phi_{0n}}{\partial y} - \frac{\partial \phi_{0n-1}}{\partial x}\right]^2 dx\,dy \Big/ \iint \left[\frac{d\phi_{0n}}{dy}\right]^2 dx\,dy. \tag{20b}$$

Convergence occurs when $\sqrt{\varepsilon_x^2 + \varepsilon_y^2} < \varepsilon$.

When $A = B$ the second order terms on the right side of Eqs. (18a) and (18b) vanish leaving only first order derivatives in v_n and u_{n+1}. This leads us to speculate that the convergence will be more rapid for problems where $A = B$. Under these condition, Eq. (1) is conveniently written as

$$\nabla \cdot (A \nabla \phi_0) = S_0. \tag{21}$$

The only numerical examples that we have considered have $A = B$.

4. Boundary Conditions

The boundary specifications for the initial equation (1) are used to generate the Poisson's equations (11a) for the series solutions or Eqs. (18a) and (18b) for the iterative solutions. If the boundary conditions for (1) are Dirichlet or Neumann, then either $\partial\phi_0/dx$ or $\partial\phi_0/dy$ are known at each boundary. If we require

$$\frac{\partial \psi_0}{\partial x} = A\frac{\partial \phi_0}{\partial x} \qquad \text{when} \quad \frac{\partial \phi_0}{\partial x} \text{ is known} \tag{22}$$

or

$$\frac{\partial \psi_0}{\partial y} = B\frac{\partial \phi_0}{\partial y} \qquad \text{when} \quad \frac{\partial \phi_0}{\partial y} \text{ is known,}$$

at a boundary, then (10) requires that

$$\frac{\partial \phi_n}{\partial x} = 0 \qquad \{n = 1, 2, 3...\} \tag{23}$$

or

$$\frac{\partial \phi_n}{\partial y} = 0 \qquad \{n = 1, 2, 3,...\}, \text{ respectively.}$$

Thus (22) and (23) are a consistent set of boundary conditions for the series solutions given by (10a), (10b), (11a), (11b), and (11c).

For the iterative solution (18a) and (18b), we require either

$$\frac{\partial u_n}{\partial x} = A \frac{\partial \phi_0}{\partial x} \qquad \text{or} \qquad \frac{\partial u_n}{\partial y} = B \frac{\partial \phi_0}{\partial y}, \tag{24}$$

consistent with the conditions at the boundaries, yielding either

$$\frac{\partial v_n}{\partial x} = 0 \qquad \text{or} \qquad \frac{\partial v_n}{\partial y} = 0, \tag{25}$$

at the boundaries, respectively.

If the boundary conditions for (1) are periodic, then the boundary conditions for the related Poisson's equations are also periodic.

For conditions of Neumann or periodic boundary conditions, if $\phi_0(x, y)$ is a solution to Eq. (1) then so is $\phi_0 + C$, where C is a constant. In order to uniquely solve Eq. (1) one must specify other conditions such as $\iint \phi_0(x, y)\, dx\, dy = 0$. The solution of all Poisson's equations in this paper are similarly restricted.

5. Application to Plasma Transport

Both the recursive series procedure and the iterative procedure have been tested numerically. We find that they are identical with respect to convergence and solution accuracy. In this section, the use of the recursive series is described in detail. The results however, are also representative of the iterative procedure.

The recursive series algorithm is tested using the transport equations for a plasma cloud in the presence of a neutral wind.

$$\frac{\partial n_e}{\partial t} - \nabla_\perp \cdot [(n_e/B_0)\, \nabla \phi_0 \times \hat{z}] = 0 \tag{26}$$

and

$$\nabla_\perp \cdot [n_e \nabla_\perp \phi_0] = (\bar{U}_n \times \bar{B}) \cdot \nabla_\perp n_e, \tag{27}$$

where n_e is the electron (or ion) concentration, $\bar{B} = B_0 \hat{z}$ is the constant magnetic field, $\bar{U}_n$ is the neutral wind velocity in the x–y plane, ϕ_0 is the electrostatic potential produced by the polarizing effects of the neutral wind, and $\nabla_\perp$ is the gradient in the x–y plane. The basis for these equations is well known (see, e.g., the reference by Ossakow *et al.* [10]). Assumptions for derivation of these equations are (1) that ion inertia can be neglected and (2) that $\nu_{in} \ll \Omega_i$, where ν_{in} is the ion neutral collision frequency and Ω_i is the ion cyclotron frequency. Such conditions are appropriate for the F-region ionosphere.

Equation (26) describes the time evolution of the electron concentration $n_e(x, y)$. Equation (26) is solved numerically using the multidimensional flux-corrected transform (FCT) algorithm described by Zalesak [15]. The potential is obtained from Eq. (27).

Equation (27) is identical to Eq. (1) with

$$A(x, y) = B(x, y) = n_e(x, y) \tag{28}$$

and

$$S_0(x, y) = (\bar{U}_n \times \bar{B}) \cdot \nabla_\perp n_e. \tag{29}$$

Equation (28) is used to simplify Eqs. (11b) and (11c) with the result

$$\frac{\partial^2 \psi_m}{\partial x^2} + \frac{\partial^2 \psi_m}{\partial y^2} = S_m \qquad \{m = 0, 1, 2, 3...\}, \tag{30a}$$

$$S_{2n} = \frac{\partial n_e}{\partial x}\frac{\partial \psi_{2n-1}}{\partial y} - \frac{\partial n_e}{\partial y}\frac{\partial \psi_{2n-1}}{\partial x}, \tag{30b}$$

and

$$S_{2n+1} = \frac{-1}{n_e^2}\left[\frac{\partial n_e}{\partial x}\frac{\partial \psi_{2n}}{\partial y} - \frac{\partial n_e}{\partial y}\frac{\partial \psi_{2n}}{\partial x}\right]. \tag{30c}$$

Many methods have been used to solve potential equations of the form given by (27). Goldman *et al.* [6] solved a linearized, small cloud approximation using double fast-Fourier transforms. Scannapieco *et al.* [11] have used iterated ADI techniques. McDonald [9] describes an explicit Chebychev-iterative solution to this type of elliptic equation. Lewis and Rehm [8] use a conjugate gradient algorithm preconditioned by a fast Poisson solver. Hain [7] uses the incomplete Cholesky-conjugate gradient (ICCG) method for the iterative solution of Eq. (27).

The method described in Section 2 provides a new approach for the solution of Eq. (27). Fast Poisson solvers such as described by Buneman [2], Buzbee *et al.* [3], Swarztrauber [12], and Sweet [14] may be used to provide solutions to (30a) with second-order or higher order accuracy. If the boundaries are doubly periodic, two dimensional fast-Fourier transforms can yield the solution to (30a).

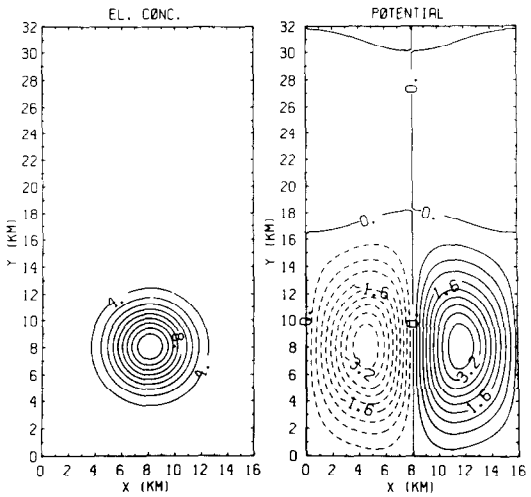

FIG. 1. Initial ($t = 0$) plasma cloud and associated electrostatic potential. The neutral wind velocity is 100 m/sec in the positive y direction. The electron concentration contours are scaled by 10^5 cm^{-3}. The potential contours are in volts. The potential was computed with the recursive series given by Eqs. (10a) and (10b) truncated to the $n = 6$ term to yield an RMS error $\varepsilon = 10^{-4}$.

Note that Eq. (26) needs only the spatial derivatives of $n(x, y)$. Consequently, the solutions in derivative form as given by Eq. (10a) and (10b) may be used directly. The potential ϕ_0 may be computed by integrating (10a) and (10b) subject to the boundary conditions. For a computational example, we consider the evolution of a plasma cloud initially described as

$$n_e(x, y) = N_0[0.3 + \exp\{-[(x - x_0)^2 + (y - y_0)^2)]/2\sigma^2\}], \tag{31}$$

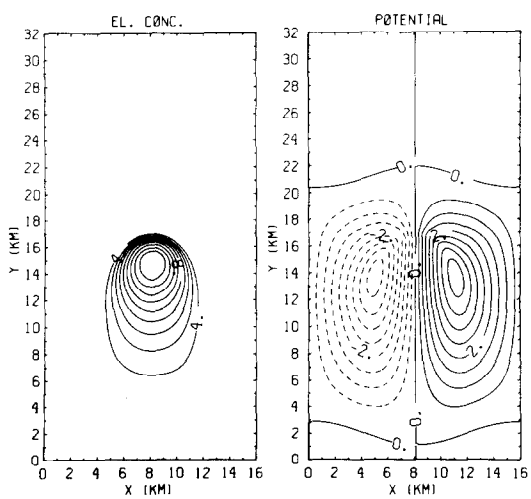

FIG. 2. Plasma cloud and electrostatic potential at time $t = 125$ sec. Scaling is the same as in Fig. 1. The recursive series for the potential is truncated at $n = 9$ for $\varepsilon = 10^{-4}$.

where $N_0 = 10^6\ e/\text{cm}^3$, $x_0 = y_0 = 8 \times 10^3$ m and $\sigma = 2 \times 10^3$ m. The cloud is subject to a $U_n = 100$ m/sec wind velocity in the y direction. The computational mesh has 64 points in the x direction ($\Delta x = 250$ m) and 128 points in the y direction ($\Delta y = 250\ m$). The boundaries are periodic in both directions. The Poisson's equations given by (30a), (30b), and (30c) are solved using the algorithms described by Swartztrauber and Sweet [13]. The Fortran coding was completely vectorized for execution on the Los Alamos CRAY1 computers.

The development of the electron concentration and the electrostatic potential is shown in Figs. 1–3. The plasma cloud moves in the y direction with a slip velocity that is 0.6 times the neutral wind velocity. The downwind side of the cloud steepens with time. The electric potential follows the motion of the cloud during its evolution. The results of these calculations are consistent with measurements of a similar plasma cloud produced by the Avefria Dos Barium experiment as reported by Fitzgerald *et al.* [5].

For this particular example, convergence is rapid. The convergence measures are given in Table I. With $\varepsilon = 10^{-4}$, the summations in Eqs. (10a) and (10b) acquire the required accuracy for $n = 6$ during the early times of the simulation. At later times, after the plasma gradients increase, convergence occurs after the $n = 11$ term is added in the series.

The growth of small scale irregularities and potentials in the cloud is illustrated by the detailed calculations of Figs. 4–6. A 1-km section of the cloud with a 1% sinusoidal perturbation is described by

$$n_e(s, y) = N_0[1 - 0.01 \sin(k_x x)]\{0.3 + \exp[(y - y_0)^2/2\sigma^2]\}, \tag{32}$$

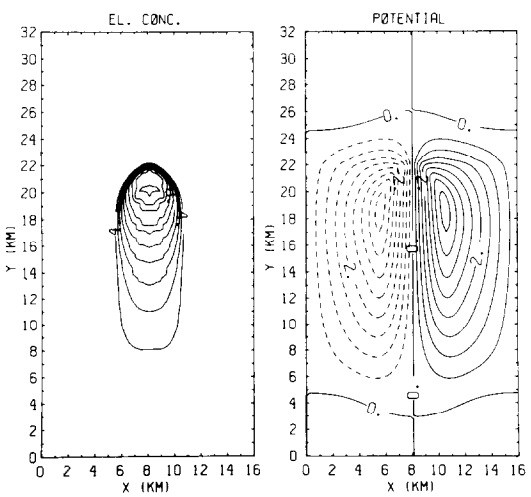

FIG. 3. Plasma cloud and electrostatic potential at $t = 220$ sec. Scaling is the same as Fig. 1. The recursive series for the potential is truncated at $n = 11$ for $\varepsilon = 10^{-4}$.

TABLE I

Convergence Parameters for Plasma Cloud Potential Computation

Time	Figure	n	ε_x	ε_y
0 sec	1	1	2.11×10^{-1}	2.21×10^{-1}
		2	3.71×10^{-2}	3.88×10^{-2}
		3	6.84×10^{-3}	7.16×10^{-3}
		4	1.25×10^{-3}	1.31×10^{-3}
		5	2.29×10^{-4}	2.40×10^{-4}
		6	4.20×10^{-5}	4.39×10^{-5}
125 sec	2	1	3.07×10^{-1}	4.06×10^{-1}
		2	8.12×10^{-2}	$1,15 \times 10^{-1}$
		3	2.46×10^{-2}	3.65×10^{-2}
		4	7.40×10^{-3}	1.12×10^{-2}
		5	2.26×10^{-3}	3.47×10^{-3}
		6	6.91×10^{-4}	1.07×10^{-3}
		7	2.12×10^{-4}	3.29×10^{-4}
		8	6.51×10^{-5}	1.01×10^{-4}
		9	2.20×10^{-5}	3.12×10^{-5}
220 sec	3	1	3.39×10^{-1}	5.59×10^{-1}
		2	1.08×10^{-1}	1.90×10^{-1}
		3	4.08×10^{-2}	7.77×10^{-2}
		4	1.52×10^{-2}	2.97×10^{-2}
		5	5.83×10^{-3}	1.16×10^{-2}
		6	2.23×10^{-3}	4.47×10^{-3}
		7	8.59×10^{-4}	1.74×10^{-3}
		8	3.31×10^{-4}	6.73×10^{-4}
		9	1.28×10^{-4}	2.61×10^{-4}
		10	4.93×10^{-5}	1.01×10^{-4}
		11	1.90×10^{-5}	3.90×10^{-5}

where $k_x = 2\pi/\lambda_x$, $\lambda_x = 10^3$ m and the remaining parameters are defined in (31). The neutral wind velocity remains at 100 m/sec. The computational mesh is 32 points in the x direction ($\Delta x = 31.25$ m) and 64 points in the y direction ($\Delta y = 187.5$ m).

Initially, the section of the plasma cloud is almost uniform in the x direction (Fig. 4). The one percent perturbation of the cloud, coupled with the neutral wind produces an electrostatic potential which is nearly uniform in the y direction. This potential stabilizes the upwind side and destabilizes the downwind side of the cloud. The convergence parameters for this computation are given in Table II. The electrostatic potential in Fig. 4 is calculated using only three terms of the recursive series. Two minutes after the start of the simulation, the amplitude of the irregularity and the magnitude of the potential on the downwind side of the cloud increase by more than a factor of 50 (Fig. 5). The potential is a dipole and the $n = 5$ term is required for its calculation with the recursive series. At $t = 155$ sec the plasma irregularity has

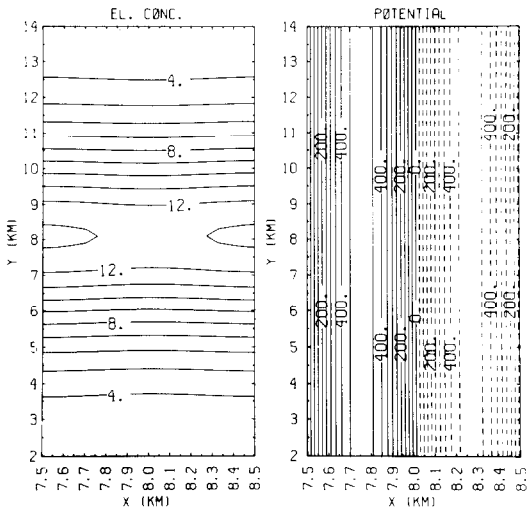

FIG. 4. Small (1%) perturbation of the plasma cloud at $t = 0$ and associated electrostatic potential. The maximum potential is 4.78×10^{-3} V. The recursive series is truncated at $n = 2$ for $\varepsilon = 10^{-4}$.

developed nonlinearly into a turbulent structure (Fig. 6). The potential has both dipole and quadrapole components. The potential for the fully developed turbulence (Fig. 6) requires only the $n = 6$ term for convergence.

The large scale motion of the plasma cloud (Figs 1–3) and the growth of small

TABLE II

Convergence Parameter for Small-Scale Potential Computations

Time	Figure	n	ε_x	ε_y
0 sec	4	1	2.18×10^{-3}	1.68×10^{-2}
		2	6.71×10^{-6}	6.85×10^{-5}
120 sec	5	1	9.60×10^{-2}	1.28×10^{-1}
		2	9.44×10^{-3}	1.48×10^{-2}
		3	9.93×10^{-4}	1.79×10^{-4}
		4	1.08×10^{-4}	2.18×10^{-4}
		5	1.21×10^{-5}	2.65×10^{-5}
155 sec	6	1	1.53×10^{-1}	1.63×10^{-1}
		2	2.15×10^{-2}	2.42×10^{-2}
		3	3.15×10^{-3}	3.86×10^{-3}
		4	4.69×10^{-4}	6.37×10^{-4}
		5	7.08×10^{-5}	1.07×10^{-5}
		6	1.09×10^{-5}	1.82×10^{-5}

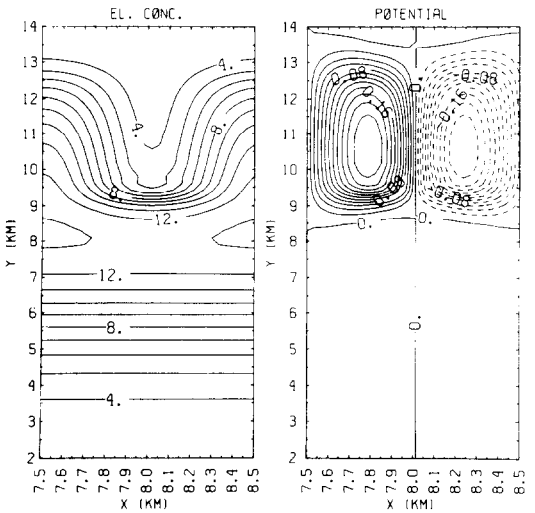

FIG. 5. Development of plasma irregularity and electrostatic potential at $t = 120$ sec. Maximum potential is 0.24 V. The recursive series is truncated at $n = 5$ for $\varepsilon = 10^{-4}$.

scale irregularities (Figs. 4–6) are both efficiently calculated with a combination of the FCT algorithm for the plasma transport and the recursive-series algorithm for the electrostatic potential. Our future numerical calculations will be directed toward the use of these algorithms for more involved treatments of plasma motion in the ionosphere.

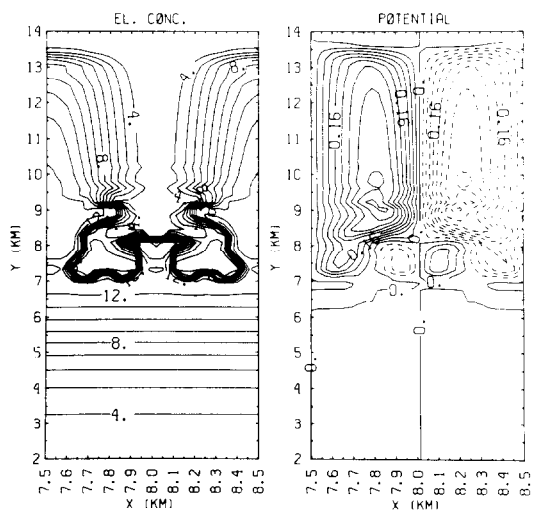

FIG. 6. Late time ($t = 155$ sec) development of plasma irregularities and electrostatic potential. Potential contours are in volts. The recursive series is truncated at $n = 6$ for $\varepsilon = 10^{-4}$.

6. Conclusions

We have shown that fast Poisson solvers can be used for the noniterative solution of the self-adjoint generalization of Poisson's equation given by (1). For the test cases we have considered, the recursive-series solution and the iterative procedure converge rapidly. For other problems, simple modifications may be necessary to insure convergence. We have shown that solvers of separable EPDEs may be applied for the solution of certain nonseparable EPDEs.

Acknowledgments

The author wishes to thank A. J. Scannapieco, V. Faber, S. P. Gary, and A. B. White, Jr. for stimulating discussions. Special acknowledgment goes to S. T. Zalesak for encouraging the writing of this paper. This work was supported by the U. S. Department of Energy.

References

1. J. U. Brackbill and D. W. Forslund, *J. Comput. Phys.* **2** (1982) 271.
2. O. Buneman, Report No. 294, Stanford University Institute for Plasma Research, Stanford, Calif., 1979.
3. B. L. Buzbee, G. H. Golub, and C. W. Nielson, *SIAM J. Numer. Anal.* **7** (1970) 627.
4. E. Detyna, Rapid elliptic solver, *in* "Sparse Matrices and Their Uses" (I. S. Duff, Ed.), Academic Press, London/New York, 1981.
5. T. J. Fitzgerald, C. F. Lebeda, M. B. Pongratz, and D. J. Simons, *Electro-Opt. Ser.* **46** (1980), 1081.
6. S. R. Goldman, S. L. Ossakow, and D. L. Brook, *J. Geophys. Res.* **79** (1974), 1471.
7. K. Hain, "A Nonrecursive Incomplete Cholesky Decomposition Method for the Solution of Linear Equations with a Sparse Matrix," NRL Memo. Rep. No. 4264. Naval Research Lab., Washington, D.C., June 16, 1980.
8. J. G. Lewis and R. G. Rehm, *J. Res. Nat. Bur. Stand.* **85** (1980), 367.
9. B. E. McDonald, "Explicit Chebychev-Iterative Solution of Nonself-adjoint Elliptic Equations on a Vector Computer," NRL Memo. Rep. No. **3541**, Naval Research Lab., Washington, D.C., June 1977.
10. S. L. Ossakow, P. K. Chaturvedi, and J. B. Workman, *J. Geophys. Res.* **83** (1978), 26101.
11. A. J. Scannapieco, S. L. Ossakow, D. L. Brook, B. E. McDonald, and S. R. Goldman, *J. Geophys. Res.* **79** (1974), 2913.
12. P. N. Swartztrauber, *SIAM J. Numer. Anal.* **12** (1974), 1236.
13. P. N. Swartztrauber and R. A. Sweet, "Efficient FORTRAN Subprograms or the Solution of Elliptic Partial Differential Equations," NCAR Tech. Note No. TN/IA-109, National Center of Atmospheric Research, Boulder, Colo. July 1975.
14. R. A. Sweet, *SIAM J. Numer. Anal.* **11** (1974), 506.
15. S. T. Zalesak, *J. Comput. Phys.* **31** (1979), 335.